

## Dielectric Response of Aligned Semiconducting Single-Wall Nanotubes

J. A. Fagan,<sup>1,\*</sup> J. R. Simpson,<sup>1</sup> B. J. Landi,<sup>2</sup> L. J. Richter,<sup>1</sup> I. Mandelbaum,<sup>1</sup> V. Bajpai,<sup>1</sup> D. L. Ho,<sup>1</sup> R. Raffaele,<sup>2</sup>  
A. R. Hight Walker,<sup>1</sup> B. J. Bauer,<sup>1</sup> and E. K. Hobbie<sup>1,†</sup>

<sup>1</sup>National Institute of Standards and Technology, Gaithersburg, Maryland 20899, USA

<sup>2</sup>NanoPower Research Laboratories, Rochester Institute of Technology, Rochester, New York 14623, USA

(Received 25 October 2006; published 6 April 2007)

We report measurements of the full intrinsic optical anisotropy of isolated single-wall carbon nanotubes (SWNTs). By combining absorption spectroscopy with transmission ellipsometry and polarization-dependent resonant Raman scattering, we obtain the real and imaginary parts of the SWNT permittivity from aligned semiconducting SWNTs dispersed in stretched polymer films. Our results are in agreement with theoretical predictions, highlighting the limited polarizability of excitons in a quasi-1D system.

DOI: [10.1103/PhysRevLett.98.147402](https://doi.org/10.1103/PhysRevLett.98.147402)

PACS numbers: 78.67.Ch, 77.22.-d, 78.20.Ci

The remarkable properties of single-wall carbon nanotubes (SWNTs) portend a number of potential applications [1]. In many of these, the ability to disperse and align individual SWNTs is critical to achieving optimal performance, as the outstanding physical attributes depend on SWNT isolation and orientation. As quasi-1D structures, the anisotropic optical and electronic characteristics of SWNTs have suggested novel opportunities in the areas of optical biological sensing [2], optoelectronics [3], conductive plastics [4], and transparent conducting films [5]. In light of this interest, a number of groups have investigated the optical anisotropy of SWNTs that have been aligned mechanically, with strong external electromagnetic fields, or through controlled growth conditions [6–12]. Such measurements offer insight into the nature of the optical transitions in SWNTs of varied diameter and chirality, but a complete picture over a broad range of the electromagnetic spectrum has yet to emerge. In particular, the polarizability of isolated semiconducting SWNTs is a critical variable in the development of schemes that use electromagnetic fields to manipulate or sort carbon nanotubes by chirality, as required for high-purity applications [13,14]. It is also central to an understanding of how SWNTs interact with light.

In this Letter, polymer composites of DNA-wrapped SWNTs in polyacrylic acid (PAA) are stretched to make transparent films of aligned SWNTs, with small-angle scattering and near-infrared fluorescence spectroscopy demonstrating ideal dispersion. The optical anisotropy of the films is measured using polarized absorption spectroscopy and transmission ellipsometry, with the SWNT alignment independently characterized by polarization-dependent resonant Raman scattering. From these measurements we extract the first measure of the complex optical response of small-diameter semiconducting nanotubes, which we find to be in agreement with theoretical predictions. Our results demonstrate the limited polarizability of excitons in semiconducting SWNTs.

Aqueous dispersion of SWNTs synthesized through the high-pressure-carbon-monoxide (HPCO) and cobalt-molybdenum-catalyst (CoMoCat) processes was achieved in the presence of 30-mer 5'-GT(GT)<sub>13</sub>GT-3' single-stranded DNA [15]. The inset of Fig. 1(a) shows a typical atomic-force microscopy (AFM) image of the DNA-coated SWNTs from dialyzed precursor suspensions. The preponderance of SWNTs are individually dispersed or in very small bundles. Polymer composites were prepared from these solutions as described elsewhere [15]. To align the SWNTs, dry films were heated to 140 °C and mechanically stretched. The composite films are optically homogeneous and transparent.

Small-angle neutron scattering (SANS) was performed on the NG7 instrument at the National Institute of Standards and Technology Center for Neutron Research. Small-angle x-ray scattering (SAXS) was performed in house using a conventional pinhole geometry. Near-infrared (NIR) fluorescence spectroscopy was performed in reflection. The incident light was vertically (*V*) polarized and the axis of mean SWNT alignment was varied by rotating the sample. UV-visible-NIR absorption spectroscopy was performed in transmission by rotating the polarizer for a fixed sample orientation. Polarization-dependent resonant Raman signal was collected in a collinear back-scattering configuration at 751.4 nm excitation. A linear vertical polarizer and analyzer were used for a *VV* configuration, with the SWNT orientation axis rotated with respect to the *V* direction. The differential anisotropy of the complex dielectric tensor for the stretched films was measured using transmission ellipsometry. In all cases, samples without SWNTs but with the same chemical and physical history were used to measure the polymer background.

Small-angle scattering is a powerful technique for measuring SWNT dispersion, since it directly probes two-point correlations in composition and can differentiate form scattering due to individual SWNTs from structural scattering due to nanotube aggregates and bundles [16–20].

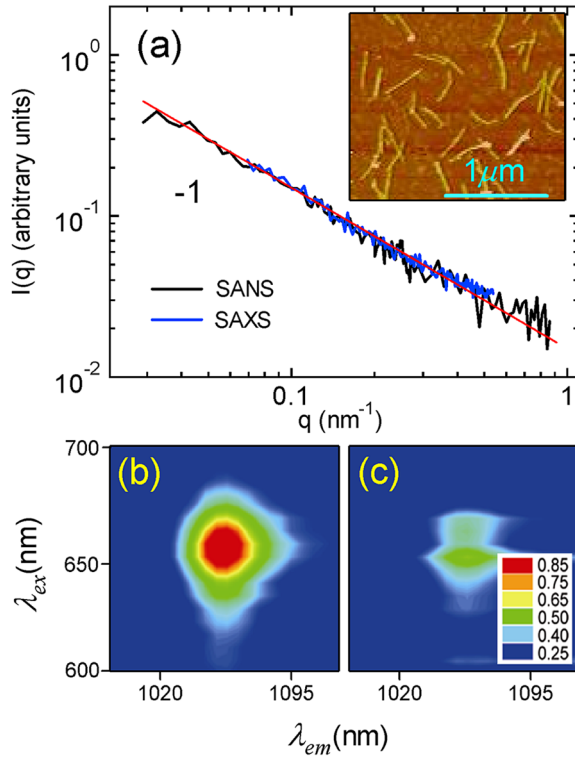


FIG. 1 (color online). (a) Background-corrected SANS and SAXS intensity versus  $q$  for an unstretched 0.035% HPCO film, where the (straight) red line is a  $-1$  power law. The inset shows an AFM image of DNA-wrapped SWNTs on mica. (b) 2D NIR fluorescence plot (excitation versus emission) for the  $(7, 5)$  SWNT feature in a stretched 0.035% CoMoCat film ( $S = 0.5$ ) with the incident light polarized along the stretch direction and (c) with the excitation polarized normal to the stretch direction.

For an isolated nanotube, the mass contained in a sphere of radius  $r$  is  $N(r) \propto r^D$ , where  $D$  is the fractal chain dimension. The radial pair-distribution function is thus  $g(r) \propto r^{1-d}(\delta N/\delta r) \propto r^{(D-d)}$ , where  $d = 3$  is the spatial dimension. Taking the Fourier transform, the scattering intensity is  $I(q) \propto q^{-D}$ , where  $q$  is the scattered wave vector. For dispersed linear objects with  $D \approx 1$ , one would therefore expect a  $q^{-1}$  power law. As shown in Fig. 1(a), unstretched composites exhibit  $q^{-1}$  behavior over a range of 6–200 nm. Since this persists up to  $q_{\max} \approx 1 \text{ nm}^{-1}$ , the diameter of the scattering objects is less than  $2\pi/q_{\max} \approx 6 \text{ nm}$ , consistent with the diameter of DNA-coated SWNTs [14].

NIR fluorescence spectroscopy provides an additional robust measure of SWNT dispersion [15]. The strength of the emission depends strongly on the polarization state of the excitation with respect to the direction of alignment [Figs. 1(b) and 1(c)], indicating a high degree of anisotropy in the films. The polymer-background-corrected absorption spectra of the stretched films show a number of well-defined peaks (Fig. 2) corresponding to SWNTs of specific chirality index  $(n, m)$ . In a single-particle excitation

scheme, these peaks reflect optical transitions between van Hove singularities above and below the Fermi level, while in a many-body picture they are necessarily excitonic in nature [21]. The absorption spectra also reveal the sensitivity of the optical transitions to polarization; absorption peaks are pronounced when the incident light is polarized parallel to the SWNT alignment axis ( $0^\circ$ ) but are suppressed normal to this direction ( $90^\circ$ ).

Alignment dependent absorption coefficients are  $a_\nu = 0.366nA_\nu\lambda/\ell\phi$ , where  $\nu$  is  $\parallel$  or  $\perp$ ,  $n$  is the index of refraction of the PAA,  $\lambda$  is the illumination wavelength,  $\ell$  is the sample thickness, and  $\phi$  is the volume fraction of SWNTs [22]. The imaginary part of the intrinsic relative permittivity along ( $\parallel$ ) and normal ( $\perp$ ) to the SWNT symmetry axis is then

$$\epsilon_{\parallel}'' = \frac{(a_{\parallel} + 2a_{\perp})S + 2(a_{\parallel} - a_{\perp})}{3S} \quad (1)$$

and

$$\epsilon_{\perp}'' = \frac{(a_{\parallel} + 2a_{\perp})S - (a_{\parallel} - a_{\perp})}{3S}, \quad (2)$$

where the nematic order parameter  $S = \langle P_2(\cos\beta) \rangle$  quantifies nanotube alignment [22]. Here,  $\beta$  denotes the angle a SWNT makes with the orientation axis,  $P_2(x)$  is the second Legendre polynomial, and  $\langle \cdot \cdot \cdot \rangle$  denotes an average over the orientational distribution  $p(\beta)$ ,  $S$  being 0 for an isotropic distribution and 1 for perfect alignment.

We obtain  $S$  from polarization-dependent resonant Raman scattering by fitting the peak intensity of the radial breathing mode (RBM) and  $G$  band as a function of  $\theta$ , the angle between the  $V$  direction and the alignment axis [Fig. 3]. The depolarized scattering intensity from a nanotube scales as  $\cos^4\psi$ , where  $\psi$  is the angle between the SWNT axis and the  $V$  direction. Expressing  $\psi$  in terms of  $\beta$  and  $\theta$ , the intensity for the ensemble is

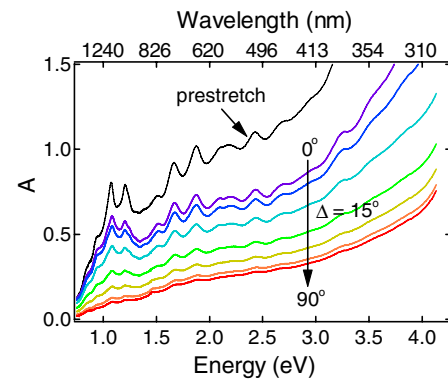


FIG. 2 (color online). UV-visible-NIR absorbance spectra as a function of photon energy and wavelength for a stretched 0.035% HPCO SWNT-PAA film ( $S = 0.8$ ), where the black trace is the prestretch absorption spectrum. The indicated angle is between the incident polarization direction and the alignment axis, where  $\Delta$  is the measurement increment.

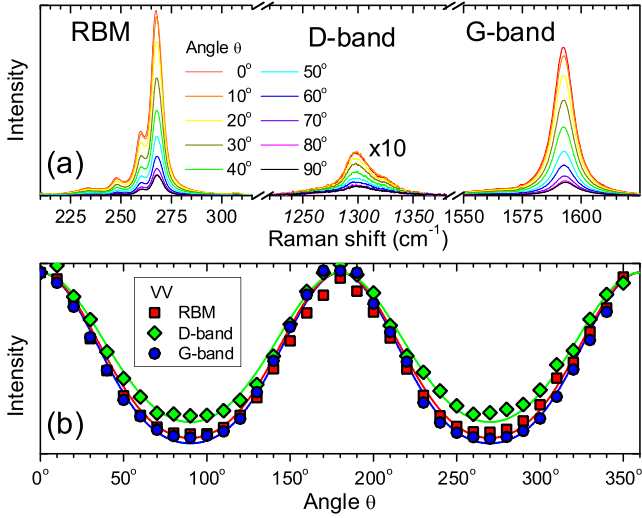


FIG. 3 (color online). (a) Polarization-dependent ( $VV$ ) resonant Raman scattering from the stretched HPCO sample in Fig. 2 (751.4 nm excitation) for the RBM,  $D$  band, and  $G$  band. (b) Angular dependence of the normalized peak intensity in (a) with fits to Eq. (3).

$$I_{vv}(\theta) \propto A \cos^4 \theta + B \cos^2 \theta \sin^2 \theta + C \sin^4 \theta, \quad (3)$$

where  $A = \langle \cos^4 \beta \rangle$ ,  $B = 3 \langle \cos^2 \beta \sin^2 \beta \rangle$ , and  $C = 3 \langle \sin^4 \beta \rangle / 8$ . Figure 3(b) shows a fit of the peak intensity from each mode to Eq. (3). From the fitting parameters  $A$ ,  $B$ , and  $C$  we obtain  $\kappa$  in the uniaxial distribution

$$p(\beta) = \frac{\kappa e^{\kappa \cos \beta}}{2\pi(e^{\kappa} - 1)} \quad (4)$$

to get  $S_{\text{RBM}} = 0.58$  and  $S_G = 0.67$  for the data depicted in Fig. 3, where the  $G$  band provides the best measure of alignment [23,24]. The  $D$  band also shows significant anisotropy ( $S_D = 0.45$ ) but does not provide a direct measure of  $S$  since one must account for the convolution of amorphous impurities. Comparable order parameters were measured for all stretched films ( $0.5 \leq S \leq 0.85$ ) with a total uncertainty of 10%.

The imaginary part of the permittivity obtained from the absorption spectra of HPCO and CoMoCat SWNTs is shown in Fig. 4. Although the anisotropy is reduced by the  $\pi$  plasmon at 4.5 eV, all absorption otherwise occurs along the length of the nanotube. For both types of SWNT, a number of semiconducting chiralities are apparent in the 11 and 22 transitions, where the relative intensity of each peak reflects content [25]. The CoMoCat sample shows a strong (6,5) enrichment. For a given  $\ell$ , transmission ellipsometry measures the difference between the dominant and minor eigenvalue of the film dielectric tensor. Dividing the imaginary part of this difference by  $S\phi$  and adding  $\epsilon''_{\perp}$  acquired from absorption provides an additional measure of  $\epsilon''_{\parallel}$  (dotted light traces in Fig. 4). Moreover, dividing the real part of this difference by  $S\phi$  provides a measure of

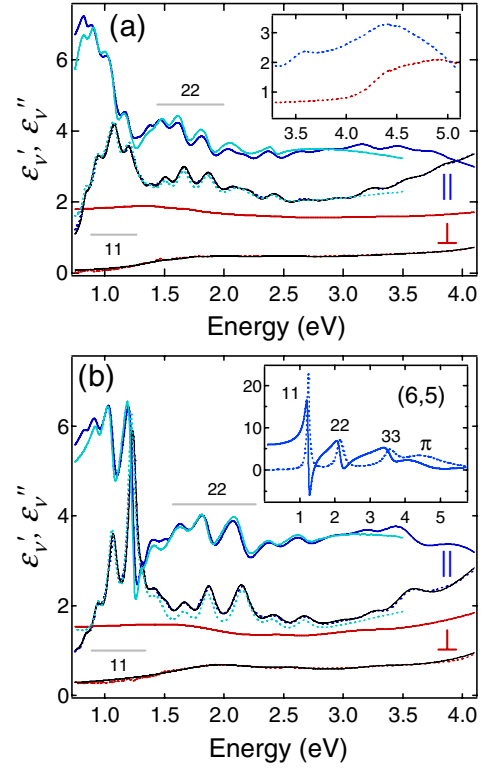


FIG. 4 (color online). (a) Intrinsic permittivity of HPCO SWNTs with a number of different chiralities evident in the  $S_{11}$  and  $S_{22}$  transitions (gray horizontal bands). Upper (lower) traces denote parallel (normal) to the SWNT symmetry axis and black curves are fits to the absorption spectra with Eq. (5). The real (imaginary) part is shown as solid (dotted) traces, where the light curves are from transmission ellipsometry. (b) An identical plot for CoMoCat SWNTs. The inset of (a) shows the anisotropy of the  $\pi$  plasmon and the inset of (b) shows the (6,5) SWNT response extracted from the fit to Eqs. (5) and (6).

$\epsilon'_{\parallel} - \epsilon'_{\perp}$ . The black traces in Fig. 4 are fits of  $\epsilon''_{\nu}$  to

$$\epsilon''_{\nu}(E) = \sum_{k=1}^{N_{\nu}} \left[ \frac{\alpha_{k,\nu} \gamma_{k,\nu}^2}{(E - E_{k,\nu})^2 + \gamma_{k,\nu}^2} - \frac{\alpha_{k,\nu} \gamma_{k,\nu}^2}{(E + E_{k,\nu})^2 + \gamma_{k,\nu}^2} \right], \quad (5)$$

with  $N_{\parallel(\perp)} = 18(6)$  and  $16(6)$  for HPCO and CoMoCat, respectively, where  $E_{k,\nu}$  is the peak position,  $\alpha_{k,\nu}$  the (dimensionless) oscillator strength, and  $\gamma_{k,\nu}$  the scattering rate associated with projection  $\nu$  of the  $k$ th peak. By analogy with the linear response of a damped harmonic oscillator, causality then gives

$$\epsilon'_{\nu}(E) = 2 \sum_{k=1}^{N_{\nu}} \frac{\alpha_{k,\nu} E_{k,\nu} \gamma_{k,\nu} (E_{k,\nu}^2 + \gamma_{k,\nu}^2 - E^2)}{(E^2 - E_{k,\nu}^2 - \gamma_{k,\nu}^2)^2 + 4\gamma_{k,\nu}^2 E^2} \quad (6)$$

to within an unknown additive constant reflecting the cut-off at 5 eV. The real part of the SWNT permittivity obtained in this manner [26] is shown as the solid curves in Fig. 4. Adding this value of  $\epsilon'_{\perp}$  to the difference  $\epsilon'_{\parallel} - \epsilon'_{\perp}$

from ellipsometry then provides a second measure of  $\epsilon'_{\parallel}$  (light solid curves in Fig. 4). The two measures of  $\epsilon'_{\nu}$  are in good agreement, giving us a self-consistent determination of the full intrinsic optical anisotropy. For a given film, the two approaches agree to within 5%, with a film-to-film variation of ca. 10%.

The presence of multiple SWNT chiralities leads to a rich landscape in the sample-averaged spectra. Our results show a reduced absorption coupled with enhanced polarizability below 1 eV (1200 nm) in the NIR. Electron-hole interactions have a profound effect on the absorption spectra of semiconducting SWNTs, giving rise to significant deviations from what one would expect based simply on the “bare” density of states [27]. Although the full optical response follows from the Kramers-Krönig relations [28], it is instructive to consider a microscopic derivation of  $\epsilon'_{\nu}$ . The predicted long-wavelength response of a bulk semiconductor is [29]

$$\epsilon'_{\nu}(0) \simeq 1 + (\hbar\omega_p/\Delta_g)^2 \{1 - O((\Delta_g/E_F)^2) + \dots\}, \quad (7)$$

where  $\omega_p$  is the plasma frequency,  $\Delta_g$  is the band gap, and  $E_F$  is the Fermi energy. This expression applies to the longitudinal SWNT response [30,31]. The inset of Fig. 4(b) shows the response of a (6, 5) SWNT extracted from the fit to Eqs. (5) and (6) in Fig. 4(b) assuming  $\phi_{(6,5)} \simeq 0.2\phi$  [32]. Accounting for electron-hole interactions [33], the empirical band gap of a (6, 5) SWNT (0.76 nm diameter) is  $\Delta_g \simeq 1.72$  eV [34]. Taking  $\omega_p$  as the position of the longitudinal  $\pi$  plasmon [13,35] and neglecting terms of  $O((\Delta_g/E_F)^2)$  then gives  $\epsilon'_{\parallel}(0) \simeq 7.5$ , from which the results in Ref. [30] suggest  $\epsilon'_{\perp}(0) \simeq 1.6$ – $1.7$ , in agreement with the data in Fig. 4.

We conclude by noting that the numbers we quote above for  $\epsilon'_{\nu}$  reflect the limited polarizability of excitons in semiconducting SWNTs. Naively using the bare computed band gap  $\Delta_g \simeq 1.1$  eV from tight-binding theory [34] gives the gross overestimate  $\epsilon'_{\parallel}(0) \simeq 17$  and  $\epsilon'_{\perp}(0) \simeq 2.6$ . In comparison, the bulk semiconductors Si and Ge have dielectric constants of 12 and 16, respectively, at 0.5 eV [36]. The relatively small measured values of SWNT dielectric constant reflect the significantly larger binding energy of optical excitations due to long-range screened Coulomb interactions in a quasi-1D system. From a computational perspective,  $\Delta_g - E_{11}$  increases significantly when electron-hole interactions are included, where  $E_{11}$  is the position of the 11 absorption peak. It is this enhanced exciton binding energy that is responsible for the reduction in polarizability; the larger the binding force the harder it is to physically separate the electron-hole pair. In this sense, our results provide an intuitive demonstration of the influence of excitons on the optical properties of semiconducting SWNTs.

\*Email address: jfagan@nist.gov

†Email address: erik.hobbie@nist.gov

- [1] See, for example, R. H. Baughman, A. A. Zakhidov, and W. A. de Heer, *Science* **297**, 787 (2002).
- [2] D. A. Heller *et al.*, *Science* **311**, 508 (2006).
- [3] M. E. Itkis *et al.*, *Science* **312**, 413 (2006).
- [4] B. Vigolo *et al.*, *Science* **309**, 920 (2005).
- [5] Z. Wu *et al.*, *Science* **305**, 1273 (2004).
- [6] W. A. de Heer *et al.*, *Science* **268**, 845 (1995).
- [7] M. Ichida *et al.*, *Appl. Phys. A* **78**, 1117 (2004).
- [8] Y. Murakami *et al.*, *Phys. Rev. Lett.* **94**, 087402 (2005).
- [9] M. F. Islam *et al.*, *Phys. Rev. Lett.* **93**, 037404 (2004).
- [10] Y. Kim, N. Minami, and S. Kazaoui, *Appl. Phys. Lett.* **86**, 073103 (2005).
- [11] M. Y. Sfeir *et al.*, *Science* **306**, 1540 (2004).
- [12] Z. M. Li *et al.*, *Phys. Rev. Lett.* **87**, 127401 (2001).
- [13] R. Krupke *et al.*, *Science* **301**, 344 (2003).
- [14] M. Zheng *et al.*, *Science* **302**, 1545 (2003).
- [15] J. A. Fagan *et al.*, *J. Phys. Chem. B* **110**, 23801 (2006).
- [16] D. Schaefer *et al.*, *J. Appl. Crystallogr.* **36**, 553 (2003).
- [17] H. Wang *et al.*, *Nano Lett.* **4**, 1789 (2004).
- [18] K. Yurekli, C. A. Mitchell, and R. Krishnamoorti, *J. Am. Chem. Soc.* **126**, 9902 (2004).
- [19] L. A. Hough *et al.*, *Nano Lett.* **6**, 313 (2006).
- [20] B. J. Bauer, E. K. Hobbie, and M. L. Becker, *Macromolecules* **39**, 2637 (2006).
- [21] F. Wang *et al.*, *Science* **308**, 838 (2005).
- [22] E. K. Hobbie, *J. Chem. Phys.* **121**, 1029 (2004).
- [23] G. S. Duesberg *et al.*, *Phys. Rev. Lett.* **85**, 5436 (2000).
- [24] A. Hartschuh *et al.*, *Phys. Rev. Lett.* **90**, 095503 (2003).
- [25] B. J. Landi *et al.*, *J. Phys. Chem. B* **109**, 9952 (2005).
- [26] The significant feature normal to the SWNT axis is the  $\pi$  plasmon and  $\epsilon'_{\perp}$  computed from  $\epsilon''_{\perp}$  is assumed robust. The known HPCO birefringence at 670 nm [ $\epsilon'_{\parallel} - \epsilon'_{\perp} \approx 1.5n_s$ , with  $n_s = 1.33$ , D. J. Fry *et al.*, *Phys. Rev. Lett.* **95**, 038304 (2005)] is then used to adjust the computed HPCO  $\epsilon'_{\parallel}$  through an additive constant, and the computed CoMoCat  $\epsilon'_{\parallel}$  is then set via invariance of the differential anisotropy at the  $\pi$  plasmon. The real part of the ellipsometry response is shifted by an additive constant reflecting the birefringence of the stretched polymer.
- [27] C. D. Spataru *et al.*, *Phys. Rev. Lett.* **92**, 077402 (2004); C. D. Spataru *et al.*, *Appl. Phys. A* **78**, 1129 (2004).
- [28] G. Y. Guo *et al.*, *Phys. Rev. B* **69**, 205416 (2004).
- [29] D. R. Penn, *Phys. Rev.* **128**, 2093 (1962).
- [30] L. X. Benedict, S. G. Louie, and M. L. Cohen, *Phys. Rev. B* **52**, 8541 (1995).
- [31] B. Kozinsky and N. Marzari, *Phys. Rev. Lett.* **96**, 166801 (2006).
- [32] Y. Oyama *et al.*, *Carbon* **44**, 873 (2006).
- [33] V. Perebeinos, J. Tersoff, and P. Avouris, *Phys. Rev. Lett.* **92**, 257402 (2004).
- [34] G. Dukovic *et al.*, *Nano Lett.* **5**, 2314 (2005).
- [35] T. Pichler *et al.*, *Phys. Rev. Lett.* **80**, 4729 (1998).
- [36] E. D. Palik, *Handbook of Optical Constants of Solids* (Academic, New York, 1985).